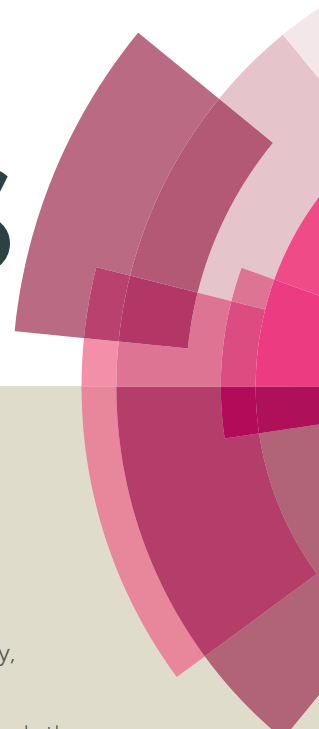


# RSC Advances



This article can be cited before page numbers have been issued, to do this please use: D. K. Chaudhary, P. Kumar and L. K. Kumar, *RSC Adv.*, 2016, DOI: 10.1039/C6RA18729C.



This is an *Accepted Manuscript*, which has been through the Royal Society of Chemistry peer review process and has been accepted for publication.

*Accepted Manuscripts* are published online shortly after acceptance, before technical editing, formatting and proof reading. Using this free service, authors can make their results available to the community, in citable form, before we publish the edited article. This *Accepted Manuscript* will be replaced by the edited, formatted and paginated article as soon as this is available.

You can find more information about *Accepted Manuscripts* in the [Information for Authors](#).

Please note that technical editing may introduce minor changes to the text and/or graphics, which may alter content. The journal's standard [Terms & Conditions](#) and the [Ethical guidelines](#) still apply. In no event shall the Royal Society of Chemistry be held responsible for any errors or omissions in this *Accepted Manuscript* or any consequences arising from the use of any information it contains.

## Evolution in surface coverage of $\text{CH}_3\text{NH}_3\text{PbI}_{3-x}\text{Cl}_x$ via Heat assisted solvent vapour treatment and their effect of device performances

Dhirendra K. Chaudhary<sup>1</sup>, Pramendra Kumar<sup>2</sup>, Lokendra Kumar<sup>1†</sup>

<sup>1</sup> Department of Physics, University of Allahabad, Allahabad-211 002, U. P., India

<sup>2</sup> Department of Applied Chemistry, IET, M. J. P. Rohilkhand University, Bareilly-243 006, U. P., India

### Abstract

We demonstrate a facile and well controlled heat assisted solvent vapour treatment (HASVT) method for the growth of compact perovskite layer with good surface coverage area in ambient atmosphere. The structural and optical properties of as deposited and solvent vapour treated films have been investigated using SEM, XRD, UV-Vis and PL spectroscopy. Furthermore, photovoltaic devices in layered configuration (FTO/TiO<sub>2</sub>/CH<sub>3</sub>NH<sub>3</sub>PbI<sub>3-x</sub>Cl<sub>x</sub>/P3HT/Ag) are fabricated using as deposited and solvent vapour treated CH<sub>3</sub>NH<sub>3</sub>PbI<sub>3-x</sub>Cl<sub>x</sub> films. The photoactive perovskite films were treated with chlorobenzene solvent vapour using HASVT method. The comparative photovoltaic performance of devices fabricated using as deposited and solvent vapour treated CH<sub>3</sub>NH<sub>3</sub>PbI<sub>3-x</sub>Cl<sub>x</sub> films was carried out. The maximum power conversion efficiency in case of vapour treatment was estimated to be ~8.05% as compared to the devices fabricated using as deposited films (~5.51%). Our systematic investigations reveal that the enhancement in power conversion efficiency is due to modification in structural and surface morphology of CH<sub>3</sub>NH<sub>3</sub>PbI<sub>3-x</sub>Cl<sub>x</sub> films.

---

<sup>†</sup> Corresponding author

Lokendra Kumar

[lokendrkr@allduniv.acinlkumarau@gmail.com](mailto:lokendrkr@allduniv.acinlkumarau@gmail.com)

## Introduction

Methyl ammonium lead halide perovskite materials has stimulated resurgence of interest for excellent light to power conversion efficiency and cost effective photovoltaic (PV) devices<sup>1,2</sup>. These perovskite photoactive materials exhibit many interesting optoelectronic properties like ambipolar charge transport, long electron-hole diffusion length and high absorption coefficient with tunable optical band gap<sup>3-6</sup>. These interesting properties may lead to a potential high efficiency solar cell device. Since last five years the organometal halide perovskite based photovoltaic technology is growing very fast and Formamidinium lead iodide (FAPbI<sub>3</sub>) based solar cells demonstrate 20% efficiency which is comparable to the commercially available silicon based solar cells<sup>7</sup>.

The power conversion efficiency of the perovskite solar cells are highly dependent on quality of films such as, surface coverage, grain size distribution, nature of crystallinity and surface morphology<sup>8-10</sup>. The control over the surface morphology is one of the major challenge in order to realize solution processed efficient perovskite solar cell<sup>11</sup>. A large volume of research have been carried out for achieving high quality perovskite films using different methods for example- mixed solvent for preparation of perovskite precursor<sup>12-14</sup>, solute composition<sup>15</sup>, using different humidity for processing<sup>16</sup>, Thermal deposition of perovskite layers<sup>1</sup>, optimization of annealing temperature and time<sup>17, 18</sup>, method of annealing<sup>19</sup>, perovskite film processing steps<sup>20</sup>, solvent treatment of perovskite layer<sup>21</sup> etc. Among them the modification in perovskite film via solvent treatment is a convenient, facile and practicable route to get control over solution processed perovskite layer. Recently, in case of DMSO solvent treatment of perovskite films, Jiang Liu *et al.* demonstrated high efficiency solar cells via engineering the crystallite size using solvent annealing method and achieved ~13 % power conversion efficiency<sup>22</sup>. Xingtian Yin *et al.* demonstrated the solution induced morphology changes in perovskite films and recorded ~13.1 % efficiency in devices with inverted architectures<sup>23</sup>. Qi Chen *et al.* developed Vapor-Assisted Solution Process (VASP) method for the growth of compact perovskite layer. This process lead modification in surface morphology as well as the device performances<sup>24</sup>. In same order Jiarong Lian *et al.* also observed the improvement in the surface morphology via organic solvent vapor treatment using DMSO and DCB as treating solvent<sup>8</sup>. Although, these treatment methods

provides better film quality of photoactive layer but shown a lack of control over solvent treatment.

Recently, we have developed an indigenous setup of heat assisted solvent vapour treatment (HASVT) for controlled solvent treatment of small molecule organic semiconducting material<sup>25</sup>. It is important to note that the adopted technique was successful in achieving controlled solvent vapour treatment that modify the ZnPc film surface roughness at nanoscale also.

Here, we demonstrate a new technique of heat assisted solvent vapour treatment (HASVT) for the manipulation of surface coverage and morphology of  $\text{CH}_3\text{NH}_3\text{PbI}_{3-x}\text{Cl}_x$  layer and get improvement in photovoltaic performance. Using this technique the improvement in the surface coverage (84.30 from 98.96 %) in relative humid environment with humidity 45 ( $\pm 2$ ) % was observed. Not only the surface modification, the larger grain boundaries (2-3  $\mu\text{m}$ ) and large crystallite size with preferential c-axis growth in perovskite films has been achieved after solvent vapour treatment.

Furthermore, perovskite solar cells was fabricated in conventional device architecture (FTO/TiO<sub>2</sub>/CH<sub>3</sub>NH<sub>3</sub>PbI<sub>3-x</sub>Cl<sub>x</sub>/P3HT/Ag) using P3HT as hole transport layer. A significant improvement (31.51 %) in the power conversion efficiency ( $\eta$  %) was achieved in the devices after solvent vapour treatment of CH<sub>3</sub>NH<sub>3</sub>PbI<sub>3-x</sub>Cl<sub>x</sub> layer as compared to as grown films. After solvent vapour treatment of CH<sub>3</sub>NH<sub>3</sub>PbI<sub>3-x</sub>Cl<sub>x</sub>films the  $\eta \sim 8.05$  % with short circuit current density ( $J_{sc}$ ) 21.37 mA/cm<sup>2</sup>, open circuit voltage ( $V_{oc}$ ) 0.8 V and fill factor 0.47 was obtained. This enhancement in device performance can be attributed to the improvement in the surface coverage, and crystalline nature of the perovskite layer after solvent vapour treatment.

## Experimental details

### Synthesis of CH<sub>3</sub>NH<sub>3</sub>I

Methyl ammonium iodide was synthesised by reacting 24 ml of methylamine (33 wt% in absolute ethanol) with 10 ml of hydroiodic acid (57 wt% in water) in 250 ml round bottom flask at 0°C for 2 h under continuous stirring. The achieved solution was put in a rotary evaporator where the solvent was evaporated at 50°C and yellowish white powder of MAI (CH<sub>3</sub>NH<sub>3</sub>I) was obtained which was re-dissolved in 80 ml of absolute ethanol and re-

precipitated by addition into 300 ml of diethyl ether. The precipitate was filtered out and the above step was repeated again for further purification. Finally a white powder of MAI was achieved which was dried in vacuum oven overnight at 70°C.

### TiO<sub>2</sub> Precursor solution preparation

TiO<sub>2</sub> precursor solution was prepared by following steps: firstly 370 μL titanium isopropoxide was drop wise added into 2.53 ml ethanol under constant stirring, keeping this solution on stirring, an another solution containing 350 μL diluted HCl (3:1) in 2.53 mL ethanol was prepared separately. This acidic solution of ethanol was mixed drop wise under constant stirring in ethanolcontaining titanium isopropoxide. The resulting solution was stirred for 30 min to yield a homogenous, clear and transparent precursor solution.

### Perovskite precursor preparation

Non-stoichiometric precursor solution of CH<sub>3</sub>NH<sub>3</sub>PbI<sub>3-x</sub>Cl<sub>x</sub> was obtained by dissolving 3:1 molar ratio of methyl ammonium iodide (MAI) to lead chloride (PbCl<sub>2</sub>) in anhydrous N,N-Dimethylformamide (DMF). The concentration of PbCl<sub>2</sub> and MAI was kept constant at 0.8 M and 2.4 M, respectively. The homogeneous precursor solution was obtained by steering precursor solution overnight at 60° C in relative humidity 45 (±2) %.

### Preparation of solar cells

FTO coated glass substrates of sheet resistivity 7-10 Ω/sq. (Sigma Aldrich) were patterned by wet etching method using HCl and Zn metal powder. Then substrates were cleaned subsequently with deionized water, acetone and isopropanol for 10 min using ultrasonic cleaner and dried in vacuum oven at 100°C for 15 min. Thereafter TiO<sub>2</sub> precursor solution was spin-coated onto pre-cleaned FTO coated glass substrates at 2000 rpm for 30 sec, the coated substrates were first dried at 100° C and then sintered at 450°C for 40 min to get TiO<sub>2</sub> compact layer.

Perovskite precursor solution was spin coated onto compact TiO<sub>2</sub> films at 5000 RPM for 20 sec. After spin coating of the perovskite layer the films were subjected to heat assisted solvent vapour treatment (HASVT). Here, the chlorobenzene organic solvent was used for the treatment of perovskite films. For solvent vapour treatment the perovskite precursor

coated substrate the film was exposed to the chlorobenzene solvent vapour for 60 sec (optimized time) by keeping the distance constant between substrate and vapour shower 10 cm and simultaneously heating the block at 80°C. After solvent vapour treatment the perovskite film annealed for 40 min at 90°C using hot plate in relative humidity 45 ( $\pm 2$ ) % to get  $\text{CH}_3\text{NH}_3\text{Pb}_{1-x}\text{Cl}_x$  film. Then Poly(3-hexylthiophene-2,5-diyl) P3HT hole transport layer was deposited onto  $\text{CH}_3\text{NH}_3\text{Pb}_{1-x}\text{Cl}_x$  layer by spin coating of solution containing 16 mg/ml P3HT in chlorobenzene at 2000 RPM for 60 sec. Then the substrates were annealed at 100°C for 5 min in vacuum oven for removal of residual solvents. Finally, 100 nm silver top electrodes was thermally deposited using cross mask at deposition rate of 0.3-0.5 Å/Sec and base pressure  $1 \times 10^{-6}$  Torr. The thickness of the deposited silver films was measured in-situ using quartz crystal thickness monitor. The active area of device prepared under cross masks was estimated to be 0.04 cm<sup>2</sup>.

### Material characterization

Surface morphology of the perovskite films were investigated using Zeiss field emission scanning electron microscope (FE-SEM). Crystalline property of the perovskite films were recorded at room temperature using Proto A-XRD diffractometer using  $\text{CuK}\alpha$  ( $\lambda = 1.054$  Å) radiation. Electronic absorption (EA) spectra of the films were obtained using Unicam 5625 UV-Vis spectrometer. Photoluminescence (PL) spectra were recorded for various samples in steady-state using Horiba Fluorolog with a 450W Xenon lamp excitation source. All spectra were corrected for instrumental response using a calibration lamp of known emissivity.

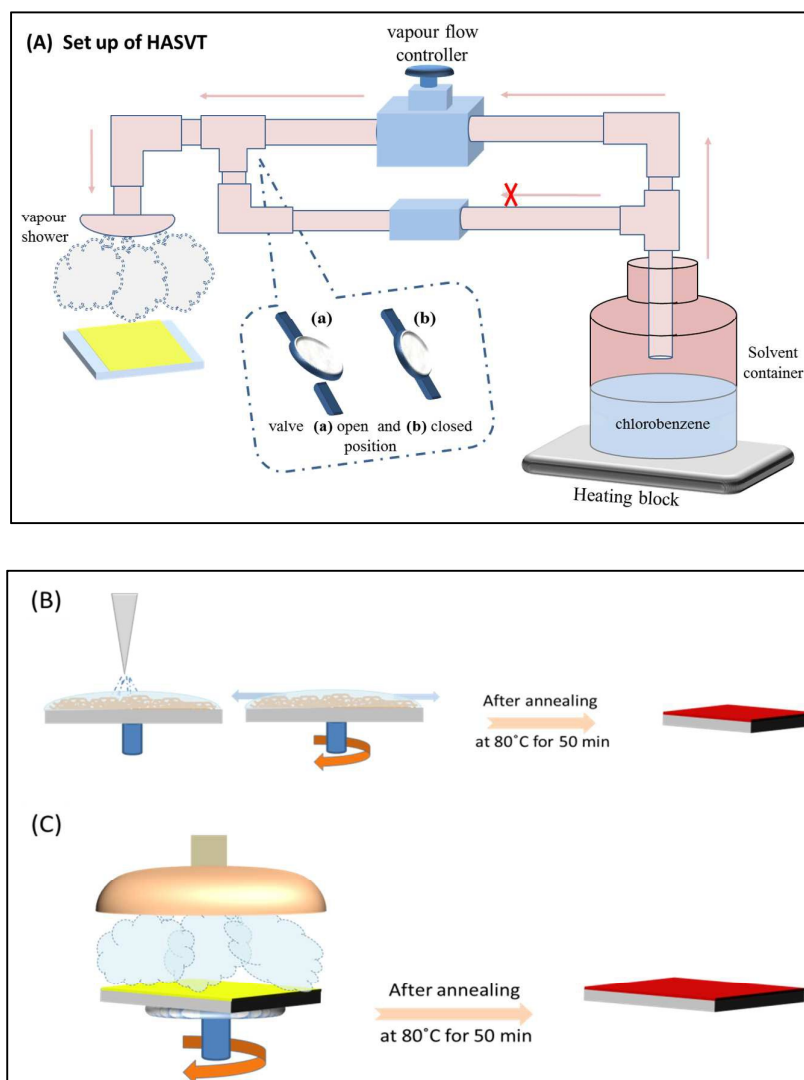
### Photovoltaic characterization

Current density–voltage (J–V) measurements were performed under simulated AM 1.5 sunlight, using Photo emission technology, USA (PET-SS50AAA-EM), a class AAA solar simulator calibrated for 100 mW cm<sup>-2</sup> light intensity (in constant intensity mode) using National Renewable Energy Laboratory (NREL) calibrated silicon reference cell. The External quantum efficiency (EQE) of the solar cells were recorded using calibrated AM 1.5G solar photon flux in the spectral range of 300 nm to 800 nm and J–V characteristics were recorded with a Keithley 2400 sourcemeter with the scanning rate of 0.285 V/s. We

observed an anomalous hysteresis effect in the devices by changing the sweep direction from -1 to +1.

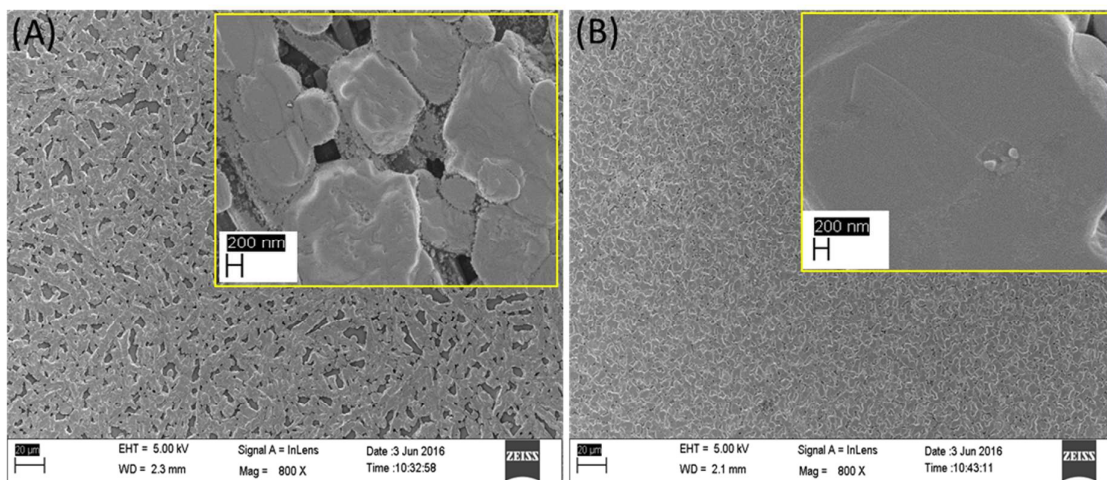
## Results and discussion

Fig. 1(A) shows the schematic diagram of heat assisted solvent vapour treatment (HASVT) setup. The setup consist of heating block, solvent container, vapour flow controller and vapour shower (porosity 0.5 mm) with pipe line of 2.4 cm inner diameter.



**Figure1:** schematic diagram of (A)heat assisted solvent vapour treatment (HASVT) set up (B) as deposited perovskite (C) solvent vapour treatment

The chemical processing of as deposited and solvent vapour treated perovskite films are shown schematically in Fig. 1 (B) & (C) , respectively.



**Figure 2:** SEM micrograph of the perovskite layers (A) as deposited (B) Solvent vapour treated

Fig. 2(a) shows the SEM micrograph of as deposited perovskite films, which shows the random distribution of perovskite grains size with some ribbon/rod like structures with large voids. The surface morphology of the as deposited perovskite films are in good agreement with report of Qing Zhou et al.<sup>17</sup> It clears from the SEM micrograph that the surface coverage of perovskite layer consists of large number of voids with different shape and size over the entire surface. The broad distribution of the perovskite grains can be clearly seen [see inset Fig. 2(a)] in the as deposited films. Fig. 2(b) shows the surface morphology of perovskite films grown using chlorobenzene solvent vapour using HASVT method. Clearly, the vapour treatment affects the surface morphology of the film. A drastic change in the surface morphology is observed and a very dense perovskite layer with grain size of 2-3 micrometres can be seen in the samples with vapour treatment [see inset Fig. 2 (b)]. Bairu Liet. al suggests that the CB vapour help DMF evaporation and accelerate the crystallization<sup>26</sup> and also the process of acceleration<sup>26</sup> via spin coating of anti-solvent is proved for one step processing of perovskite films<sup>27, 28</sup>. So, in case of samples with vapour treatment, the observed modification in morphology could be due to acceleration in recrystallization process of perovskite films.

The surface coverage of perovskite layer has been estimated via ImageJ program using threshold function<sup>29</sup> at different location and magnification of the SEM images. The estimated value of surface coverage for as deposited and solvent vapour treated  $\text{CH}_3\text{NH}_3\text{PbI}_{3-x}\text{Cl}_x$  films are 84.30% and 98.98%, respectively. These results provide strong evidence that the good quality of  $\text{CH}_3\text{NH}_3\text{PbI}_{3-x}\text{Cl}_x$  films could be achieved through chlorobenzene solvent vapour treatment using HASTV method.

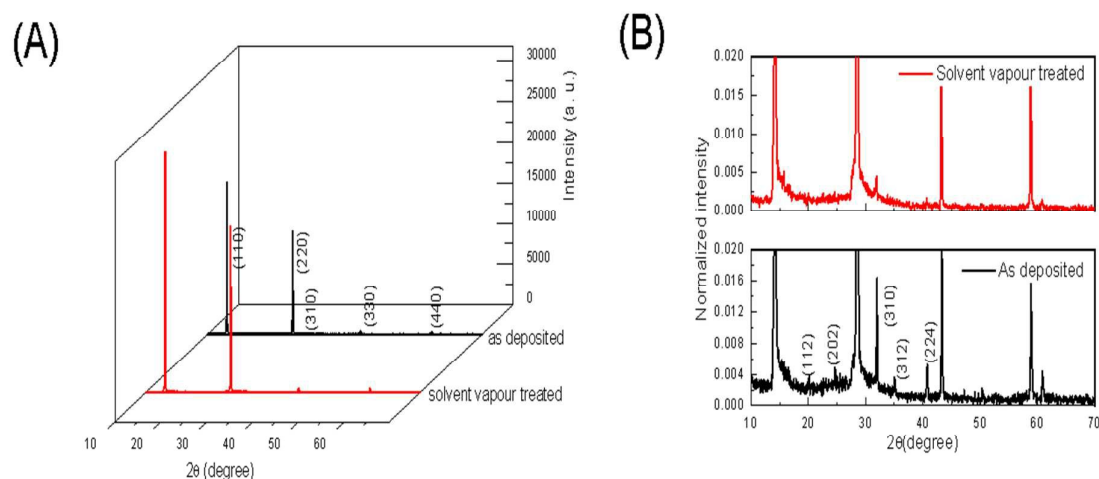


**Figure 3:** (A) The absolute and (B) normalized XRD pattern of as deposited, solvent treated and solvent vapour treated  $\text{CH}_3\text{NH}_3\text{PbI}_{3-x}\text{Cl}_x$  films.

Fig 3(A) shows the XRD pattern of as deposited and solvent vapour treated  $\text{CH}_3\text{NH}_3\text{PbI}_{3-x}\text{Cl}_x$  films. The diffractions peaks at position 14.1, 28.4, 31.83, 43.2 and 58.9  $2\theta$  degree positions are assigned to the planes of (110), (220), (310), (330) and (440) tetragonal crystal structure of  $\text{CH}_3\text{NH}_3\text{PbI}_3$ . It is interesting to note that no additional peak of  $\text{PbI}_2$  or  $\text{CH}_3\text{NH}_3\text{I}$  has been observed which suggests that the entire surface covered with crystalline  $\text{CH}_3\text{NH}_3\text{PbI}_{3-x}\text{Cl}_x$  only. The intensity of the characteristic peak for solvent treated  $\text{CH}_3\text{NH}_3\text{PbI}_{3-x}\text{Cl}_x$  film are found to be significantly enhanced in comparison to the as grown samples. A small variation in the FWHM of the prominent peaks corresponding to plane (110) and (220) is observed, which varied from 0.062 to 0.053 and 0.0680 to 0.0602, respectively. The mean coherent scattering domain size of crystallites were calculated using Debye–Scherrer

formula and found to be 130 nm and 150 nm for as deposited and solvent vapour treated  $\text{CH}_3\text{NH}_3\text{PbI}_{3-x}\text{Cl}_x$  films respectively. The change in FWHM and enhancement in the intensity of the peak profile may be due to larger crystallite size and dense perovskite layer after solvent treatment [see Fig. 2 (B)]. To take insight look of XRD data, the normalized XRD data plots corresponding to peak at position  $14.2^\circ$   $2\theta$  value has been shown in fig. 2(B). The enlarge plot shows some other peaks of very small intensity in as deposited films and chlorobenzene solution treated films. Interestingly, the relative intensity of peak at position 20.04, 24.64, 31.95, 35.09, 40.69 and 60.84 have diminished in solvent vapour treated  $\text{CH}_3\text{NH}_3\text{PbI}_{3-x}\text{Cl}_x$  films which suggest that highly oriented crystal domains formation of  $\text{CH}_3\text{NH}_3\text{PbI}_{3-x}\text{Cl}_x$  form solvent vapour treatment.

Note that the surface modification using other techniques like thermal solvent annealing, and solvent treatment method changes the surface morphology of the films but these techniques are not able to change the crystallite size. The modification in crystallite size after chlorobenzene treatment has been discussed by JiarongLian et al<sup>8</sup>.

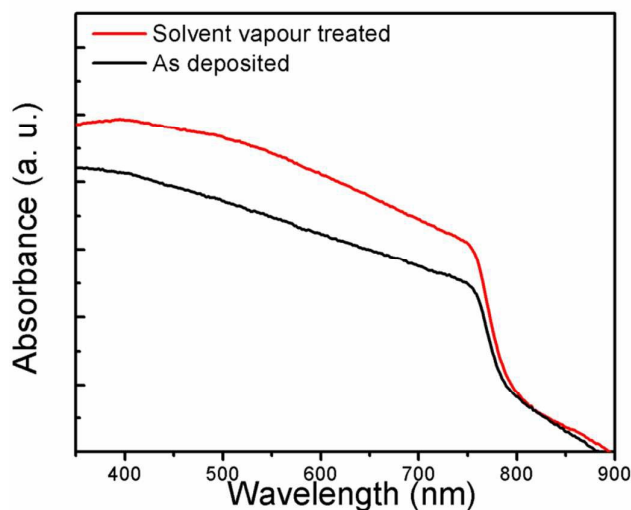


**Figure 4:** UV-Vis absorption spectra of as deposited and solvent vapour treated  $\text{CH}_3\text{NH}_3\text{PbI}_{3-x}\text{Cl}_x$  films

Fig. 4 shows the UV-Vis. absorption spectra of the  $\text{CH}_3\text{NH}_3\text{PbI}_{3-x}\text{Cl}_x$  films under different processing conditions. The absorption spectra of  $\text{CH}_3\text{NH}_3\text{PbI}_{3-x}\text{Cl}_x$  films show the good coverage of solar spectrum from band gap  $\sim 1.57$  eV [calculated from Tauc Plot] with

considerably sharp absorption edge. Also, the absorption profile that the solvent vapour treated  $\text{CH}_3\text{NH}_3\text{PbI}_{3-x}\text{Cl}_x$  samples shows more absorbance in comparison to as grown samples. The sharper absorption edge and enhanced absorbance could be due to combined effect of well-defined crystal morphology, high degree of crystallinity and good surface coverage of the  $\text{CH}_3\text{NH}_3\text{PbI}_{3-x}\text{Cl}_x$  films.

It is possible that the larger grain size may leads enhancement in the absorbance of vapour treated films. The large grain size increases the distance of light propagation due to back scattering of incident light from the comparatively rough surface<sup>30-32</sup>.

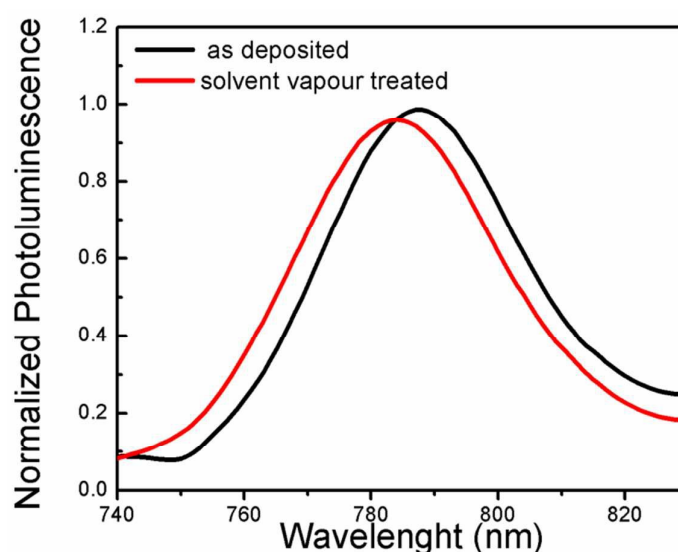


**Figure 5:** Photoluminescence spectra of perovskite films processed under different conditions

Fig. 5 shows the normalized steady state Photoluminescence (PL) emission spectra of  $\text{CH}_3\text{NH}_3\text{PbI}_{3-x}\text{Cl}_x$  films on glass substrate under different processing conditions. PL of the films was recorded by using the excitation wavelength near the absorption band edge. The  $\text{CH}_3\text{NH}_3\text{PbI}_{3-x}\text{Cl}_x$  sample without any treatment shows the PL emission peak at 787 nm, which shows good agreement with previous reported data<sup>33</sup>. After HASVT treatment of the film the PL peak blue shifted as compared to the as deposited film and appeared at 783 nm. A negligibly small change in the FWHM of the PL peak has been observed before and after the treatment. In general the PL emission is related to the recombination channels concerning the band gap and trap state<sup>22</sup>. The observed blue shift with reduced FWHM of PL

emission of perovskite films could be due to reduction of trap density near the band edge. The reduction in trap density could be due to larger grain size.

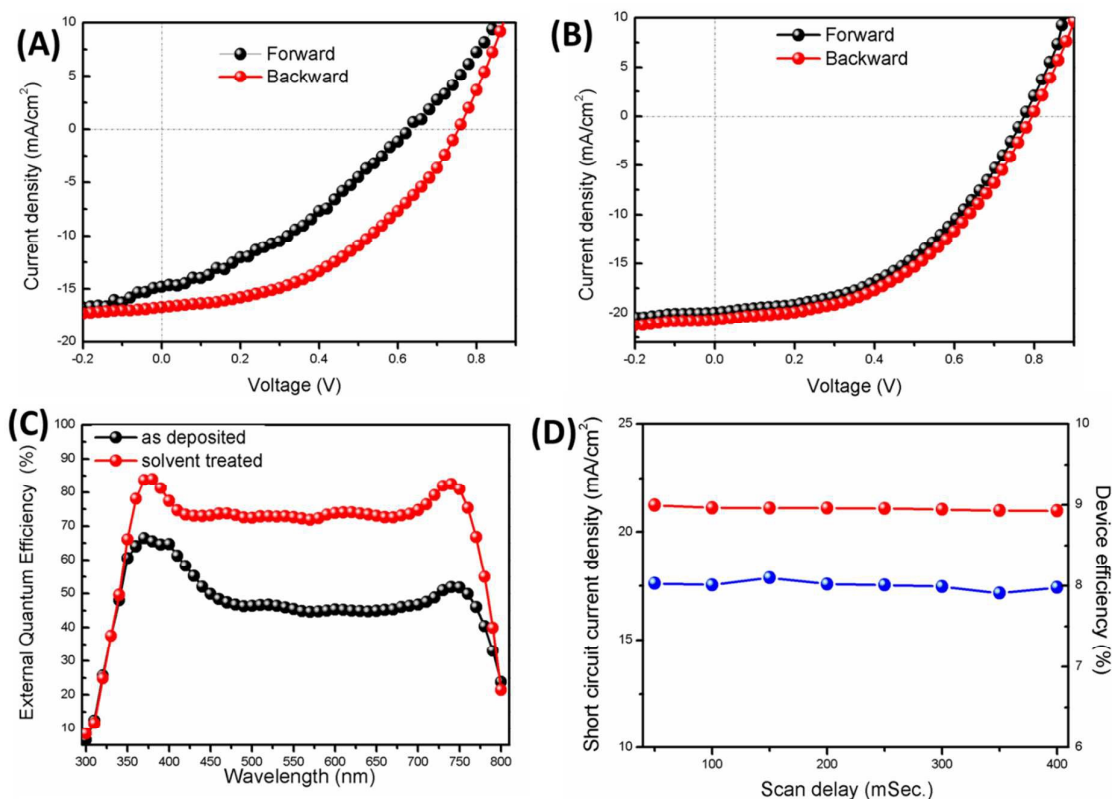


**Figure 6:** J-V characteristics of device fabricated with (A) as deposited (B) solvent vapour treated  $\text{CH}_3\text{NH}_3\text{PbI}_{3-x}\text{Cl}_x$  films and (C) External Quantum efficiency spectra (D)  $J_{SC}$  and  $\eta$  with different scan delay.

Fig. 6 (A) and (B) shows the  $J$ - $V$  characteristics in forward and backward scan direction of our best performing devices, fabricated using as deposited and HASVT films, respectively. The photovoltaic performances of the devices are shown in table 1. The devices fabricated using  $\text{CH}_3\text{NH}_3\text{PbI}_{3-x}\text{Cl}_x$  film without any treatment shows  $\eta \sim 3.26\%$  and  $\sim 5.51\%$  in forward and backward scan respectively, which is in good agreement with others reports of devices fabricated in ambient atmosphere. Interestingly, the enhancement in the power conversion efficiency up to  $\eta \sim 7.38\%$  (in forward scan) and  $\sim 8.1\%$  (in backward scan) is reached in the devices when we use vapour treatment to the perovskite films. The scan direction dependent behaviour in the device is due to existence of anomalous hysteresis<sup>34, 35</sup>. Sufficiently high hysteresis has been observed in  $J$ - $V$  curve of devices fabricated with as

deposited perovskite layer. Whereas, significant passivation in anomalous hysteresis of J-V characteristics is observed in solvent vapour treated devices.

Device		$J_{sc}(mA/cm^2)$	$V_{oc}(V)$	$FF$	$\eta \%$
<b>As deposited</b>	Forward scan	14.63	0.62	0.36	3.26
	Backward scan	16.70	0.74	0.44	5.51
<b>Solvent Vapour Treated</b>	Forward scan	20.03	0.79	0.46	7.38
	Backward scan	21.37	0.80	0.47	8.05

**Table 1:** Photovoltaic performance of the devices fabricated with as deposited and solvent vapour treated  $CH_3NH_3PbI_{3-x}Cl_x$  films.

To compare the hysteresis in both devices the hysteresis index (HI) has been estimated using hysteresis index formula reported by R. S. Sanchez et al.<sup>36</sup> and shown in equation (1).

$$\text{hysteresis index} = \frac{J_{BS}(0.5V_{OC}) - J_{FS}(0.5V_{OC})}{J_{BS}(0.5V_{OC})} \dots (1)$$

Where  $J_{FS}(0.5V_{OC})$  and  $J_{BS}(0.5V_{OC})$  stands for value of photocurrent density at 50 % of  $V_{OC}$  for forward and backward scan respectively. The value of  $HI = 0$  corresponds to a device without observable hysteresis, while  $HI = 1$  corresponds to such type of devices which possess hysteresis as high as the photocurrent<sup>36</sup>. Using equation (1) we estimated the value of  $HI$  in both devices and found to be  $\sim 0.440$  and  $\sim 0.036$  for devices fabricated with as deposited and solvent vapour treated perovskite films respectively. Here, we observed a twelve fold reduce in  $HI$  after solvent vapour treatment. This reduced anomalous hysteresis attributes could be due to the reduction in trap states which causes due to formation compact perovskite films with larger grain size. Whereas the residual hysteresis in J-V characteristics of solvent treated devices may be due to ferroelectric properties<sup>35</sup>, electro migration of ions or some other factors. Fig. 6(C) shows the external quantum efficiency (EQE) spectrum of the both devices. The EQE curve starts increasing near 800 nm in both spectra which is in good agreement with electronic absorption of  $CH_3NH_3PbI_{3-x}Cl_x$ . A

broad plateau of  $\sim 78\%$  ( $\pm 2\%$ ) in entire visible region is observed in the EQE curve of device fabricated with solvent vapour treated perovskite films. To check the reproducibility of the data, we recorded EQE of the four devices and observed almost same profile of EQE spectrum with small variation. The integrated  $J_{SC}$  value was estimated theoretically and found to be  $\sim 19.21 \text{ mA/cm}^2$ . Estimated value of  $J_{SC}$  is very close to experimentally observed value of  $J_{SC}$ . The observed slightly lower value of current density from EQE may be due the surface trap of the  $\text{TiO}_2$  electron transporting layer<sup>24</sup>. Whereas the estimated value of current density is found to be  $\sim 12.59 \text{ mA/cm}^2$  of device fabricated using perovskite films without treatment. A large difference in calculated and experimentally observed value of EQE is observed in the devices fabricated without treatment. This difference may be due to the capacitance of the devices<sup>38</sup>. The plot of Power conversion efficiency and  $J_{SC}$  of the devices fabricated with solvent vapour treated perovskite films with different delay time are shown in fig. 6 (D). Almost delay independent behaviour in device performance is observed. Whereas J-V characteristics of the devices fabricated using without treated perovskite films are highly dependent on scan delay time (data not shown).

Figure 7 shows the efficiency histogram plot of 20 devices fabricated using as deposited and solvent vapour treated perovskite films respectively, keeping same processing parameters conditions at same lab conditions. A wide range distribution in efficiency of the devices fabricated using as deposited perovskite films is observed. This wide range distribution efficiency could be due to unequal distribution of perovskite layer. Whereas 95 % of devices shows efficiency very close to best performing device after HASVT of perovskite films. These results show that the device performance quit consistent and reproducible after solvent vapour treatment. This consistency and reproducibility in devices are result of compact perovskite films.

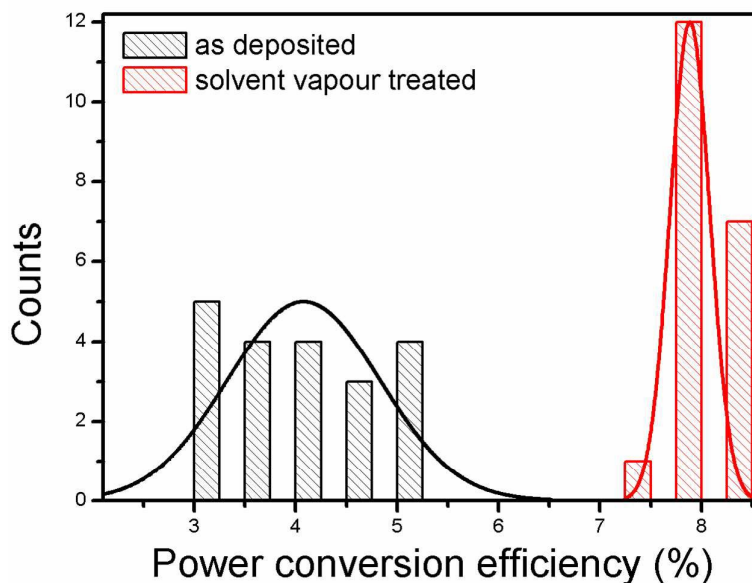


**Figure 7:** Histogram of power conversion efficiency of devices fabricated as deposited and solvent vapour treated  $\text{CH}_3\text{NH}_3\text{PbI}_{3-x}\text{Cl}_x$  films.

The devices fabricated using HASVT treated  $\text{CH}_3\text{NH}_3\text{PbI}_{3-x}\text{Cl}_x$  films shows power conversion efficiency up to  $\eta \sim 8.05\%$  with reduced anomalous hysteresis. The performances of devices are reproducible and consistent. Note that, these films are fabricated in the ambient atmosphere without any lithographic and glove box fabrication processes. The better photovoltaic performance in vapour treatment of the  $\text{CH}_3\text{NH}_3\text{PbI}_{3-x}\text{Cl}_x$  layer is attributed to the larger grain size and surface coverage. It could be possible that the larger grain sizes reduce the recombination centres (trap level) and grain boundaries which reduce possibility of electron and hole recombination processes as a result of photon excitation. So the larger grain size, compact perovskite layer and enhanced absorbance of the  $\text{CH}_3\text{NH}_3\text{PbI}_{3-x}\text{Cl}_x$  all these collectively contributed to enhance power conversion efficiency by the devices fabricated with solvent vapour treated  $\text{CH}_3\text{NH}_3\text{PbI}_{3-x}\text{Cl}_x$  films.

## Conclusions

The heat assisted solvent vapour treatment (HASVT) method has been demonstrated for uniform growth of perovskite layer. A systematic investigation on structural and optical properties of perovskite layer has been carried out. Our results suggest that the larger surface coverage and grain size can be obtained in  $\text{CH}_3\text{NH}_3\text{PbI}_{3-x}\text{Cl}_x$  layer by HASVT method. These parameter results the blue shift in the PL spectra of the solvent vapour treated

CH<sub>3</sub>NH<sub>3</sub>PbI<sub>3-x</sub>Cl<sub>x</sub>films. Photovoltaic performances of devices fabricated with as deposited and films grown with HASVT methods were compared. An enhancement of 33.51% has been achieved in the devices fabricated using films grown with the HASVT methods. Our results provide strong evidence that the HASVT method could be potential techniques for the growth of the high quality active layer for PV devices.

## Acknowledgements

The financial support to this work was provided by the Department of Science & Technology under FTP grant number SERB/F/5521 and DST-FIST grants. We thank P. Kumar, CSIR-NPL, New Delhi for Perovskite materials and other supports during this work. Author(s) acknowledge Rahul and R. K. Gupta, Chemical Engineering Department, IIT, Kanpur, India, for his kind help in EQE measurements.

## References

1. M. Liu, M. B. Johnston and H. J. Snaith, *Nature*, 2013, **501**, 395-398.
2. M. M. Lee, J. Teuscher, T. Miyasaka, T. N. Murakami and H. J. Snaith, *Science*, 2012, **338**, 643-647.
3. M. A. Green, A. Ho-Baillie and H. J. Snaith, *Nature Photonics*, 2014, **8**, 506-514.
4. G. E. Eperon, S. D. Stranks, C. Menelaou, M. B. Johnston, L. M. Herz and H. J. Snaith, *Energy & Environmental Science*, 2014, **7**, 982-988.
5. N. J. Jeon, J. H. Noh, Y. C. Kim, W. S. Yang, S. Ryu and S. I. Seok, *Nature materials*, 2014, **13**, 897-903.
6. H. J. Snaith, *The Journal of Physical Chemistry Letters*, 2013, **4**, 3623-3630.
7. W. S. Yang, J. H. Noh, N. J. Jeon, Y. C. Kim, S. Ryu, J. Seo and S. I. Seok, *Science*, 2015, **348**, 1234-1237.
8. J. Lian, Q. Wang, Y. Yuan, Y. Shao and J. Huang, *Journal of Materials Chemistry A*, 2015, **3**, 9146-9151.
9. J. Xing, X. F. Liu, Q. Zhang, S. T. Ha, Y. W. Yuan, C. Shen, T. C. Sum and Q. Xiong, *Nano letters*, 2015, **15**, 4571-4577.
10. J. Chen, T. Shi, X. Li, B. Zhou, H. Cao and Y. Wang, *Applied Physics Letters*, 2016, **108**, 053302.
11. Q. Chen, H. Zhou, Z. Hong, S. Luo, H.-S. Duan, H.-H. Wang, Y. Liu, G. Li and Y. Yang, *Journal of the American Chemical Society*, 2014, **136**, 622-625.
12. H.-B. Kim, H. Choi, J. Jeong, S. Kim, B. Walker, S. Song and J. Y. Kim, *Nanoscale*, 2014, **6**, 6679-6683.
13. C. D. Chandler, C. Roger and M. J. Hampden-Smith, *Chemical Reviews*, 1993, **93**, 1205-1241.
14. P. W. Liang, C. Y. Liao, C. C. Chueh, F. Zuo, S. T. Williams, X. K. Xin, J. Lin and A. K. Y. Jen, *Advanced Materials*, 2014, **26**, 3748-3754.
15. J. Qing, H.-T. Chandran, Y.-H. Cheng, X.-K. Liu, H.-W. Li, S.-W. Tsang, M.-F. Lo and C.-S. Lee, *ACS applied materials & interfaces*, 2015, **7**, 23110-23116.
16. J. Yang, B. D. Siempelkamp, D. Liu and T. L. Kelly, *ACS Nano*, 2015, **9**, 1955-1963.
17. Q. Zhou, Z. Jin, H. Li and J. Wang, *Scientific reports*, 2016, **6**.

18. A. Dualeh, N. Tétreault, T. Moehl, P. Gao, M. K. Nazeeruddin and M. Grätzel, *Advanced Functional Materials*, 2014, **24**, 3250-3258.
19. F. X. Xie, D. Zhang, H. Su, X. Ren, K. S. Wong, M. Grätzel and W. C. Choy, *ACS nano*, 2015, **9**, 639-646.
20. H.-L. Hsu, C.-P. Chen, J.-Y. Chang, Y.-Y. Yu and Y.-K. Shen, *Nanoscale*, 2014, **6**, 10281-10288.
21. N. J. Jeon, J. H. Noh, Y. C. Kim, W. S. Yang, S. Ryu and S. I. Seok, *Nat Mater*, 2014, **13**, 897-903.
22. J. Liu, C. Gao, X. He, Q. Ye, L. Ouyang, D. Zhuang, C. Liao, J. Mei and W. Lau, *ACS Applied Materials & Interfaces*, 2015, **7**, 24008-24015.
23. X. Yin, M. Que, Y. Xing, X. Liu, W. Que and C. Niu, *Electrochimica Acta*, 2016, **191**, 750-757.
24. Q. Chen, H. Zhou, Z. Hong, S. Luo, H.-S. Duan, H.-H. Wang, Y. Liu, G. Li and Y. Yang, *Journal of the American Chemical Society*, 2013, **136**, 622-625.
25. D. K. Chaudhary and L. Kumar, *Journal of Materials Science: Materials in Electronics*, 2016, DOI: 10.1007/s10854-016-5170-5, 1-6.
26. B. Li, T. Jiu, C. Kuang, S. Ma, Q. Chen, X. Li and J. Fang, *Organic Electronics*, 2016, **34**, 97-103.
27. M. Xiao, F. Huang, W. Huang, Y. Dkhissi, Y. Zhu, J. Etheridge, A. Gray-Weale, U. Bach, Y.-B. Cheng and L. Spiccia, *Angewandte Chemie*, 2014, **126**, 10056-10061.
28. N. Ahn, D.-Y. Son, I.-H. Jang, S. M. Kang, M. Choi and N.-G. Park, *Journal of the American Chemical Society*, 2015, **137**, 8696-8699.
29. W. Rasband, *US National Institutes of Health*, 2005.
30. N. Cheng, P. Liu, S. Bai, Z. Yu, W. Liu, S.-S. Guo and X.-Z. Zhao, *Journal of Power Sources*, 2016, **319**, 111-115.
31. Y. Xie, F. Shao, Y. Wang, T. Xu, D. Wang and F. Huang, *ACS Applied Materials & Interfaces*, 2015, **7**, 12937-12942.
32. T. Zhang, M. Yang, Y. Zhao and K. Zhu, *Nano Letters*, 2015, **15**, 3959-3963.
33. C. Wehrenfennig, M. Liu, H. J. Snaith, M. B. Johnston and L. M. Herz, *The Journal of Physical Chemistry Letters*, 2014, **5**, 1300-1306.
34. E. L. Unger, E. T. Hoke, C. D. Bailie, W. H. Nguyen, A. R. Bowring, T. Heumuller, M. G. Christoforo and M. D. McGehee, *Energy & Environmental Science*, 2014, **7**, 3690-3698.
35. H. J. Snaith, A. Abate, J. M. Ball, G. E. Eperon, T. Leijtens, N. K. Noel, S. D. Stranks, J. T.-W. Wang, K. Wojciechowski and W. Zhang, *The Journal of Physical Chemistry Letters*, 2014, **5**, 1511-1515.
36. R. S. Sanchez, V. Gonzalez-Pedro, J.-W. Lee, N.-G. Park, Y. S. Kang, I. Mora-Sero and J. Bisquert, *The Journal of Physical Chemistry Letters*, 2014, **5**, 2357-2363.
37. Y. Shao, Z. Xiao, C. Bi, Y. Yuan and J. Huang, *Nature communications*, 2014, **5**.
38. B. Chen, M. Yang, X. Zheng, C. Wu, W. Li, Y. Yan, J. Bisquert, G. Garcia-Belmonte, K. Zhu and S. Priya, *The Journal of Physical Chemistry Letters*, 2015, **6**, 4693-4700.